Ambipolar surface state transport in nonmetallic stoichiometric Bi$_2$Se$_3$ crystals

Paul Syers and Johnpierre Paglione[*]

Center for Nanophysics and Advanced Materials, Department of Physics, University of Maryland, College Park, Maryland 20742, USA
(Received 20 July 2015; revised manuscript received 28 October 2016; published 17 January 2017)

Achieving true bulk insulating behavior in Bi$_2$Se$_3$, the archetypal topological insulator with a simplistic one-band electronic structure and sizable band gap, has been prohibited by a well-known self-doping effect caused by selenium vacancies, whose extra electrons shift the chemical potential into the bulk conduction band. We report a synthesis method for achieving stoichiometric Bi$_2$Se$_3$ crystals that exhibit nonmetallic behavior in electrical transport down to low temperatures. Hall-effect measurements indicate the presence of both electron- and holelike carriers, with the latter identified with surface state conduction and the achievement of ambipolar transport in bulk Bi$_2$Se$_3$ crystals without gating techniques. With carrier mobilities surpassing the highest values yet reported for topological surface states in this material, the achievement of ambipolar transport via upward band bending is found to provide a key method to advancing the potential of this material for future study and applications.

I. INTRODUCTION

The development of topological insulator (TI) materials has found rapid progress in the past few years [1]. Distinguished from ordinary insulators by the so-called Z$_2$ topological invariants associated with the bulk electronic band structure [2,3], this class of materials is characterized by nonlocal topology of the electronic structure that gives rise to new electronic states with promise for realizing new technologies such as fault-tolerant quantum computation [4]. By far the most widely studied system within the field of TI research is Bi$_2T_3$ ($T =$ Se,Te) [5–10]. To date, the major experimental efforts on these noninteracting bismuth-based TI materials have focused on refining measurement techniques in order to detect signatures of surface states. However, a continuing problem with the stoichiometric materials lies in the fact that they are not bulk insulators as predicted but rather doped semiconductors [11]. Both the bulk and surface quality of TI materials are known to dramatically affect their properties, with the effects of site exchange (e.g., in Bi$_2$Te$_3$) or Se vacancy doping (e.g., in Bi$_2$Se$_3$) serving to introduce excess charge carriers in the bulk (n-type with Bi$_2$Se$_3$ and p-type with Bi$_2$Te$_3$), reduce surface carrier mobilities, and mix bulk and surface state conduction contributions.

The common method of crystal growth using excess selenium falls short of reaching even a nonmetallic temperature dependence of resistivity [12], which has to date produced samples with some of the lowest bulk carrier concentrations ever reported. Extensive work has been carried out to suppress bulk conductivity contributions by compensation doping [7,8,13–15], but this has only been achieved in the binary materials by introducing excess impurity scattering via chemical substitution methods [16,17], such as was accomplished using Se-Te site substitution in the case of the ternary compound Bi$_2$Te$_2$Se [18,19]. Synthesis of defect-free epitaxial thin films [20,21] has also succeeded in reducing conduction through the bulk, and electrostatic gating techniques have been used to lower the chemical potential (E_F) into the bulk-band-gap

regime [22–24]. But sensitivity to environmental conditions and crystalline quality [12] continue to pose problems for Bi$_2$Se$_3$. This ultimately requires complicated and nuanced analysis of experimental data to identify and study the intrinsic nature of the topologically protected surface states, no matter the sample size; in the absence of further progress, increased attention is being devoted to other classes of materials [25–28].

Here we employ a high-pressure bulk crystal growth technique to demonstrate the lowest attained bulk carrier concentrations in stoichiometric Bi$_2$Se$_3$, achieving a regime of nonmetallic transport behavior. Observations of a nonlinear Hall coefficient clearly identify the presence of two carrier types that can only be identified with separate bulk and surface state contributions to conductivity, with the coexistence of positive and negative carriers providing unequivocal proof of TI surface states from transport data alone.

II. METHODS

Single crystals of Bi$_2$Se$_3$ were grown under high gas pressures from ultrapure ($\geqslant$99.999%) elemental Bi and Se via a self-flux technique [12], utilizing a high-pressure containment vessel. (See further details of the growth procedure in the Supplemental Material [29].) All crystals were in the size range 0.5–1 mm width and 1–2 mm length, with $\sim$50-μm thickness. Longitudinal and Hall resistance measurements were performed simultaneously on all samples reported here, using a six-wire configuration with two voltage contacts in standard longitudinal configuration and two voltage contacts in a transverse (Hall) configuration, both sharing the same current contacts. All samples were measured in a commercial cryostat as a function of temperatures between 2 and 300 K and magnetic fields up to $\pm$14 T.

III. RESULTS

The temperature dependence of the resistivity $\rho(T)$ shown in Fig. 1 illustrates the range of nonmetallic behavior of three samples of Bi$_2$Se$_3$ crystals grown using the high-pressure technique. Two additional samples, V and H, are included for comparison. Sample H shows the metallic behavior typical
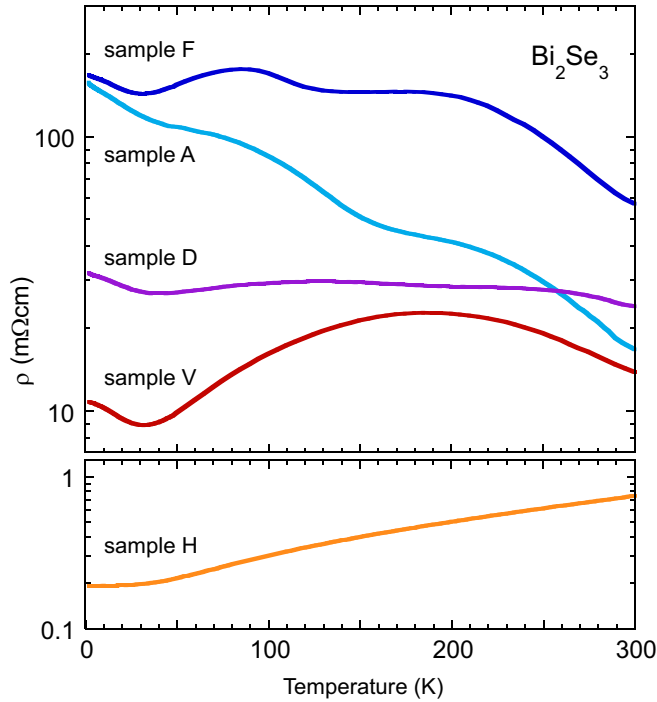
---

*paglione@umd.edu

FIG. 1. Electrical resistivity of stoichiometric Bi_2Se_3 crystals with varying carrier concentrations resulting from variations in sample growth conditions. Samples A, F, and D all show an overall increase in ρ between 300 K and 2 K. Samples V and H, shown for comparison, have semimetallic and metallic behavior.

FIG. 2. Analysis of quantum oscillations observed in Bi_2Se_3 sample H, a high-carrier-density crystal. Panel (a) presents the background-subtracted longitudinal resistance as a function of inverse magnetic field, with a fitted model (solid line) that incorporates the presence of two oscillation frequencies (85 T and 95 T) with a 1.24π phase shift between them. Panel (b) presents a plot of the Hall resistivity for the same sample measured *in situ*, along with a two-carrier model fit shown as a solid line. The resultant carrier densities and mobilities are shown in the inset, with carrier densities that match the values expected for the two oscillation frequencies noted above (see text for details).

of most samples of Bi_2Se_3 in the literature, while sample V shows semimetallic behavior identical to other low-carrier-concentration pure samples reported to date [11,12].

Unlike samples V and H, the nonmetallic crystals (A, D, F) exhibit an overall increase in resistivity with decreasing temperature. Furthermore, the most insulating samples exhibit a room-temperature resistivity value far greater than the comparison samples or previous measurements of both pure and chemically substituted samples of Bi_2Se_3 [12,16,17], indicating that the insulating behavior originates mainly from a clear decrease in overall carrier density (as opposed to a strong increase in scattering rate). The presence of a distinct minimum in resistivity near 30 K in all samples follows the concentration-independent trend reported previously [11,12] and is consistent with a phonon-dependent scattering feature [30] that only changes with lattice density such as induced by external pressure, which readily pushes the minimum up in temperature [31]. This is also true for pure surface state transport, as reported for crystals gated into the bulk gap [32]. Interestingly, the appearance of an unusual double-hump structure in the resistivity of most nonmetallic samples (i.e., samples A and F) seems to be a continuous extension of the ~200 K maximum and ~30 K minimum observed very clearly in slightly more metallic samples (i.e., sample V). While Shubnikov–de Haas (SdH) oscillations can be discerned in low-temperature (2 K) magnetoresistance measurements of samples V and H, they are absent in the measurements of the nonmetallic samples, indicating that the bulk carriers are at a low enough concentration to be in the quantum limit at moderate fields.
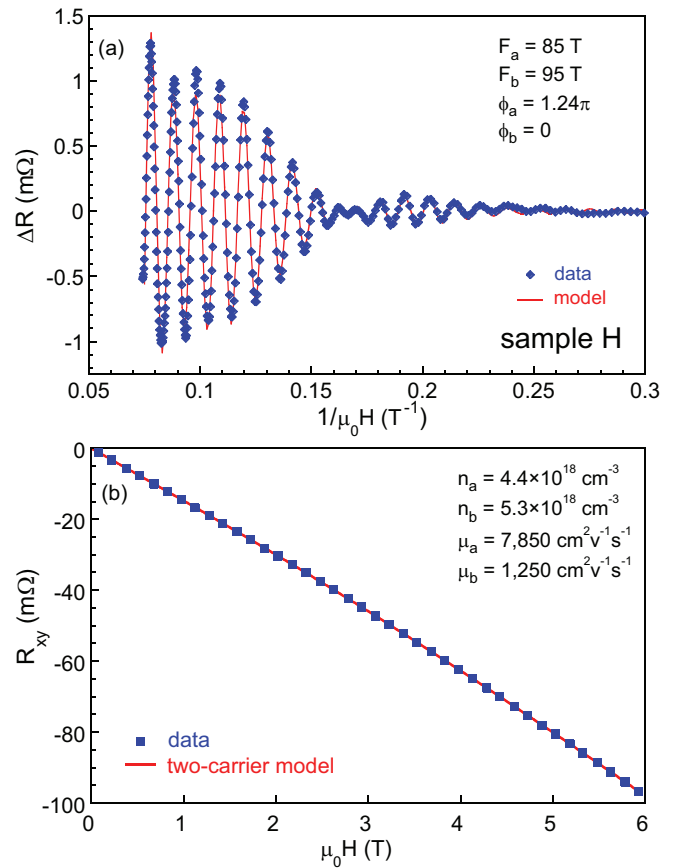
A two-carrier Drude model was used to fit the Hall effect data for all samples, assuming two carriers of the same sign (electronlike) for samples D, V, and H and two with different sign carriers (one electron- and one holelike) for samples A and F, respectively. Together with self-consistent fits to low-field ($\leqslant 1$ T) longitudinal magnetoresistance (see SM [29]), a best match for the four physical parameters (density and mobility for each carrier) was reached for each of the nonmetallic samples. To independently verify the fitting procedure, we first compare such results to analysis of SdH oscillations observable in higher-carrier-density samples. Samples V and H both exhibit SdH oscillations, as usual for moderately doped samples [12], but the latter sample exhibits a rare case of two oscillatory components, as clearly observable in the beating modulation presented in Fig. 2(a). Fourier transform analysis confirms two oscillation frequencies of 85 T and 95 T, corresponding to three-dimensional carrier densities of 4.4×10^{18} cm^{-3} and 5.3×10^{18} cm^{-3}, respectively. This
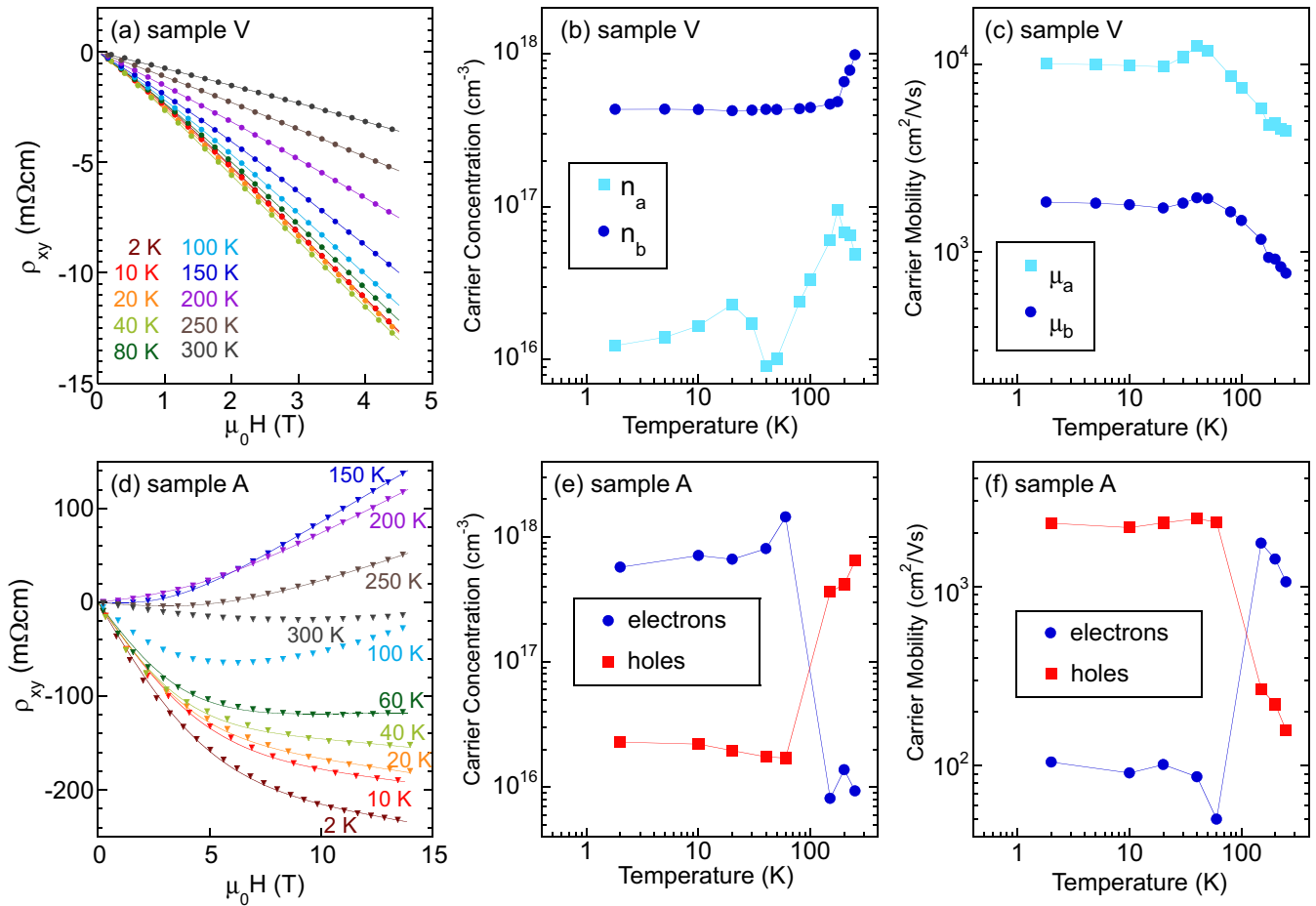
FIG. 3. Hall-effect data and analysis of single-crystal Bi₂Se₃ obtained for two characteristic samples V and A, shown in panels (a–c) and (d–f), respectively. Transverse Hall resistance is presented in panels (a) and (d), with Drude model fits (see text) shown as solid lines. Panels (b) and (e) present the carrier densities extracted from the two-carrier analysis, and panels (c) and (f) present the resultant mobilities for each carrier type. The presence of two carrier contributions is easily discerned by the nonlinear behavior of $\rho_{xy}(H)$, in particular for sample A, which presents a crossover from electron- to hole-dominated conduction as a function of temperature. As described in the text, the two carrier types are ascribed to bulk and surface state carriers present in each sample, with holelike conduction necessarily originating from surface states in sample A.

compares perfectly with the concentrations extracted from Hall data shown in Fig. 2(b).

Applying the standard Lifschitz-Kosevich formalism with an assumed typical effective mass of $0.1m_e$ [12], we model the oscillations of samples V and H and extract Dingle temperatures and phase (ϕ) information for the oscillations in both samples. From the analysis, carrier mobilities also compare favorably between SdH and Drude transport fit results (see SM [29] for details). More surprising, for both samples the extracted ϕ values for the two oscillatory components are considerably offset (by nearly π) from one another This is extraordinary, considering that quantum oscillations of surface states in Bi₂Se₃ have so far only been observed in very high (pulsed) magnetic fields in samples with enhanced bulk scattering [17]. In the case of sample H, the corresponding mobility is much enhanced for the component with relative phase shift, approaching a value of 7850 cm² V⁻¹ s⁻¹ as obtained by Drude analysis.

Using the same Drude analysis, we now compare Hall effect measurements and extracted mobility and carrier densities of semimetallic sample V [Figs. 3(a)–3(c)] to those of the much

more nonmetallic sample A [Figs. 3(d)–3(f)], which does not exhibit any observable trace of quantum oscillations. As shown, the Hall resistivities (ρ_{xy}) exhibit very unusual behavior with respect to magnetic field and temperature, especially in light of the well-characterized, single-band electronic structure of Bi₂Se₃ [5]. Hall data for sample V is nearly linear but exhibits a small but pronounced curvature in $\rho_{xy}(H)$ indicative of the presence of more than one type of charge carrier. Sample A, with more pronounced nonmetallic behavior in $\rho(T)$, also exhibits much more pronounced nonlinearity in $\rho_{xy}(H)$, even crossing over to a holelike response as temperature is raised.

The extracted mobility μ and carrier concentration n values for each carrier type are shown in Figs. 3(c)–3(f). Surprisingly, the electron carrier density $n_e = 4.3 \times 10^{17}$ cm⁻³ of sample A at 2 K is found to be higher than both carrier concentrations extracted from sample-V data. However, the corresponding electron mobility is found to be extremely low [Fig. 3(f)], accounting for the lack of observable quantum oscillations in this sample. The high mobilities of the minor bands in both samples are what account for their signatures in the

Hall curves. Interestingly, the comparable values of mobilities of the lower carrier bands (approaching 8000 cm^2 V^{-1} s^{-1}) with those found in sample H is intriguing and suggestive of similar scattering processes. Most important, such large values are notably higher than any reported in the literature thus far, including those of molecular-beam-epitaxy–grown thin films with atomically sharp epitaxial interfaces [33–35]. This is an interesting observation, especially considering the rather strict limit imposed by electron-phonon scattering studied previously [32], suggesting that the current result may exemplify the ultimate limit of surface mobilities.

Given the extensive efforts to increase mobilities of surface carriers through such efforts, it is important to investigate the manner by which this is achieved and to understand why perfecting crystal quality and/or suppressing the bulk carrier concentration is not sufficient. The most striking result of the Hall analysis is the clear evidence of two carrier types, and moreover, evidence for two carriers with opposite signs in select samples. Bi$_2$Se$_3$ p-type samples have been previously reported [11], but the recent extensive set of measurements [5,36–43] studying the electronic structure of Bi$_2$Se$_3$ have verified that its band structure is simplistic and includes only one bulk conduction and valence band together with Dirac surface states that cross the insulating gap. Therefore the most likely origin of the two carrier types is from bulk- and surface-derived bands. For two electronlike carriers (as for sample V), contributions from bulk and surface bands are understandable but one must also consider other causes, such as spin-split bulk bands [42,43] and trapped quantum well states due to downward band bending at the surface of the crystal [44–46]. However, the observation of holelike carriers uniquely rules out such situations and allows for only one explanation: upward band bending. *This is the key aspect of achieving high surface state mobility.*

Using carrier densities estimated from Hall data analysis to calculate the corresponding two- and three-dimensional Fermi momenta k_F for each sample, we map the positions of the surface and bulk chemical potentials onto the band structure measured by photoemission [47], as shown in Fig. 4. In line with previous studies [11,12], the bulk band E_F always appears to remain pinned to the edge of the conduction band and cannot be pushed into the gap for bulk samples by growth techniques alone. However, as shown, the surface E_F energies are distributed over a wider range, and even traverse the Dirac point. In our study, they do tend to remain close to the Dirac point, which may result from charge puddling [23] that acts to pin the surface E_F there. The energy spacing between surface and bulk E_F values indicate band bending of up to 190 meV, with the stronger band bending occurring in the more insulating samples and, most important, resulting in a hole-type carrier contribution to total conduction. While the direction of the band bending at the surface of Bi$_2$Se$_3$ is almost universally reported to be downward, most studies have been performed either on thin-film samples or high-carrier-density samples. One previous study performed on lower-carrier-density samples (i.e., comparable to sample V) has indeed reported upward band bending [37], possibly arising from surface-based interactions with elemental selenium. The suppression of selenium vapor pressure by the pressurized
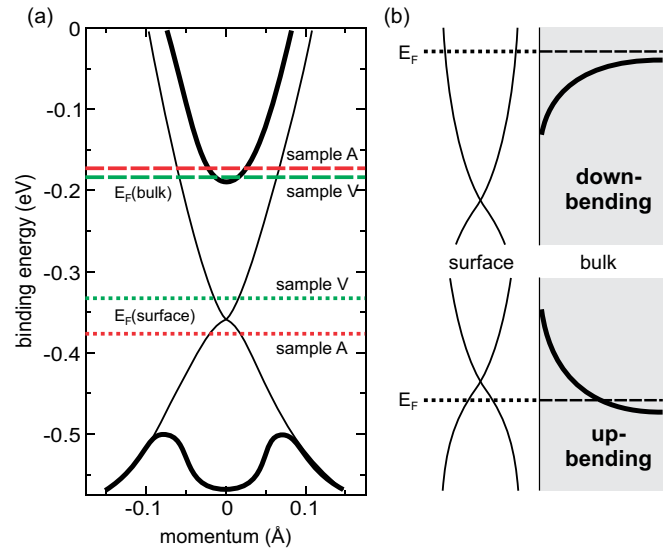

FIG. 4. (a) Electronic band structure of Bi$_2$Se$_3$ obtained from photoemission experiments [44], showing the positioning of bulk (dashed lines) and surface (dotted lines) chemical potential values E_F extracted from two-carrier analysis of data for samples A and V (see text). Panel (b) presents a schematic of the difference between downward and upward band bending near the surface, providing an explanation for the positioning of surface chemical potentials of samples V and A near the Dirac point, consistent with an upward-band-bending picture.

inert gas environment used in our crystal growth method may invoke a similar mechanism.

IV. SUMMARY

An upward band bending that places the surface chemical potential near the Dirac point yields the only plausible scenario that provides hole-type carriers in this band structure. Controlling the level of bending by growth tuning provides the ability to tune the position of the surface potential to be either above or below the Dirac point, demonstrating ambipolar transport of the Dirac surface states in large single crystals, an effect previously achieved only via gating techniques applied to ultrathin films or samples [23]. The significant enhancement in the measured TI surface state mobilities in stoichiometric Bi$_2$Se$_3$ is surprising in comparison to prior extensive work on this material and points to the importance of this material preparation technique that yields the uncommon band-bending effect. This is confirmed by our observations of changes in the transport data as a function of time (see SM [29]). The suppression of resistivity values with air exposure time, in particular, in the most insulating samples that exhibit hole-type behavior, is consistent with a significant downward shift in the energy bands at the surface, in agreement with previous studies of the electronic structure evolution at the surface of Bi$_2$Se$_3$ [38,48]. Furthermore, the model of Se buildup at the surface of samples causing upward band bending is supported by findings that the carrier concentrations in samples increase with mechanical exfoliation [23,49].

Overall, while complete bulk insulating behavior in stoichiometric Bi$_2$Se$_3$ remains difficult to achieve, our

observations of greatly enhanced mobilities and ambipolar transport without atomically perfect thin films or fabricated gate structures suggests that engineering of electronic band bending near the surface of crystals via new routes of materials synthesis and preparation promises a route to optimizing use of the simplest three-dimensional topological insulator.

[1] M. Z. Hasan and C. L. Kane, Rev. Mod. Phys. **82**, 3045 (2010).

[2] C. L. Kane and E. J. Mele, Phys. Rev. Lett. **95**, 146802 (2005).

[3] L. Fu and C. L. Kane, Phys. Rev. B **74**, 195312 (2006).

[4] C. Nayak, S. H. Simon, A. Stern, M. Freedman, and S. D. Sarma, Rev. Mod. Phys. **80**, 1083 (2008).

[5] Y. Xia, D. Qian, D. Hsieh, L. Wray, A. Pal, H. Lin, A. Bansil, D. Grauer, Y. S. Hor, R. J. Cava, and M. Z. Hasan, Nat. Phys. **5**, 398 (2009).

[6] H. Zhang, C. X. Liu, X. L. Qi, X. Dai, Z. Fang, and S. C. Zhang, Nat. Phys. **5**, 438 (2009).

[7] Y. L. Chen, J. G. Analytis, J.-H. Chu, Z. K. Liu, S.-K. Mo, X. L. Qi, H. J. Zhang, D. H. Lu, X. Dai, Z. Fang, S. C. Zhang, I. R. Fisher, Z. Hussain, and Z.-X. Shen, Science **325**, 178 (2009).

[8] Y. L. Chen, J. H. Chu, J. G. Analytis, Z. K. Liu, K. Igarashi, H. H. Duo, X. L. Qi, S. K. Mo, R. G. Moore, D. H. Lu, M. Hashimoto, T. Sasagawa, S. C. Zhang, I. R. Fisher, Z. Hussain, and Z. X. Shen, Science **329**, 659 (2010).

[9] H.-C. Liu, H.-Z. Lu, H.-T. He, B. Li, S.-G. Liu, Q. L. He, G. Wang, I. K. Sou, S.-Q. Shen, and J. Wang, ACS Nano **8**, 9616 (2014).

[10] P. Deorani, J. Son, K. Banerjee, N. Koirala, M. Brahlek, S. Oh, and H. Yang, Phys. Rev. B **90**, 094403 (2014).

[11] H. Köhler and A. Fabricius, Phys. Status Solidi B **71**, 487 (1975).

[12] N. P. Butch, K. Kirshenbaum, P. Syers, A. B. Sushkov, G. S. Jenkins, H. D. Drew, and J. Paglione, Phys. Rev. B **81**, 241301 (2010).

[13] Y. S. Hor, J. G. Checkelsky, D. Qu, N. P. Ong, and R. J. Cava, J. Phys. Chem. Solids **72**, 572 (2011).

[14] Y. S. Hor, A. Richardella, P. Roushan, Y. Xia, J. G. Checkelsky, A. Yazdani, M. Z. Hasan, N. P. Ong, and R. J. Cava, Phys. Rev. B **79**, 195208 (2009).

[15] D. Hsieh, Y. Xia, D. Qian, L. W. J. H. Dil, F. Meier, J. Osterwalder, L. Patthey, J. G. Checkelsky, N. P. Ong, A. V. Fedorov, H. Lin, A. Bansil, D. Grauer, Y. S. Hor, R. J. Cava, and M. Z. Hasan, Nature (London) **460**, 1101 (2009).

[16] J. G. Checkelssky, Y. S. Hor, M.-H. Liu, D.-X. Qu, R. J. Cava, and N. P. Ong, Phys. Rev. Lett. **103**, 246601 (2009).

[17] J. G. Analytis, R. D. McDonald, S. C. Riggs, J.-H. Chu, G. S. Boebinger, and I. R. Fisher, Nat. Phys. **6**, 960 (2010).

[18] Z. Ren, A. A. Taskin, S. Sasaki, K. Segawa, and Y. Ando, Phys. Rev. B **82**, 241306(R) (2010).

[19] L. Barreto, L. Khnemund, F. Edler, C. Tegenkamp, J. Mi, M. Bremholm, B. B. Iversen, C. Frydendahl, M. Bianchi, and P. Hofmann, Nano Lett. **14**, 3755 (2014).

[20] Y. Y. Li, G. Wang, X. G. Zhu, M. H. Liu, C. Ye, X. Chen, Y. Y. Wang, K. He, L. L. Wang, X. C. Ma, H. J. Zhang, X. Dai, Z. Fang, X. C. Xie, Y. Liu, X. L. Qi, J. F. Jia, S. C. Zhang, and Q. K. Xue, Adv. Mater. **22**, 4002 (2010).

[21] M. Brahlek, Y. S. Kim, N. Bansal, E. Edrey, and S. Oh, Appl. Phys. Lett. **99**, 012109 (2011).

[22] S. Cho, N. P. Butch, J. Paglione, and M. S. Fuhrer, Nano Lett. **11**, 1925 (2011).

[23] D. Kim, S. Cho, N. P. Butch, P. Syers, K. Kirshenbaum, S. Adam, J. Paglione, and M. S. Fuhrer, Nat. Phys. **8**, 459 (2012).

[24] H. Steinberg, J.-B. Lalo, J. S. Moodera, and P. Jarillo-Herrero, Phys. Rev. B **84**, 233101 (2011).

[25] B. Yan, H.-J. Zhang, C.-X. Liu, X.-L. Qi, T. Frauenheim, and S.-C. Zhang, Phys. Rev. B **82**, 161108 (2010).

[26] M. Dzero, K. Sun, V. Galitski, and P. Coleman, Phys. Rev. Lett. **104**, 106408 (2010).

[27] H. Lin, L. A. Wray, Y. Xia, S. Xu, S. Jia, R. J. Cava, A. Bansil, and M. Z. Hasan, Nat. Mater. **9**, 546 (2010).

[28] S. Chadov, X. Qi, J. Kbler, G. H. Fecher, C. Felser, and S. C. Zhang, Nat. Mater. **9**, 541 (2010).

[29] See Supplemental Material at http://link.aps.org/supplemental/10.1103/PhysRevB.95.045123 for further details of the growth procedure.

[30] M. Stordeur, K. K. Ketavong, A. Priemuth, H. Sobotta, and V. Riede, Phys. Status Solidi B **169**, 505 (1992).

[31] J. J. Hamlin, J. R. Jeffries, N. P. Butch, P. Syers, D. A. Zocco, S. T. Weir, Y. K. Vohra, J. Paglione, and M. B. Maple, J. Phys.: Condens. Matter **24** 035602 (2012).

[32] D. Kim, Q. Li, P. Syers, N. P. Butch, J. Paglione, S. D. Sarma, and M. S. Fuhrer, Phys. Rev. Lett. **109**, 166801 (2012).

[33] H. D. Li, Z. Y. Wang, X. Kang, X. Guo, H. T. He, Z. Wang, J. N. Wang, T. L. Wong, N. Wang, and M. H. Xie, New J. Phys. **12**, 103038 (2010).

[34] A. Richardella, D. M. Zhang, J. S. Lee, A. Koser, D. W. Rench, A. L. Yeats, B. B. Buckley, D. D. Awschalom, and N. Samarth, Appl. Phys. Lett. **97**, 262104 (2010).

[35] M. T. Edmonds, J. T. Hellerstedt, A. Tadich, A. Schenk, K. M. O'Donnell, J. Tosado, N. P. Butch, P. Syers, J. Paglione, and M. S. Fuhrer, ACS Nano **8**, 6400 (2014).

[36] C. Jozwiak, Y. L. Chen, A. V. Fedorov, J. G. Analytis, C. R. Rotundu, A. K. Schmid, J. D. Denlinger, Y.-D. Chuang, D.-H. Lee, I. R. Fisher, R. J. Birgenau, Z.-X. Shen, Z. Hussain, and A. Lanzara, Phys. Rev. B **84**, 165113 (2011).

[37] J. G. Analytis, J.-H. Chu, Y. Chen, F. Corredor, R. D. McDonald, Z. X. Shen, and I. R. Fisher, Phys. Rev. B **81**, 205407 (2010).

[38] D. Kong, J. J. Cha, K. Lai, H. Peng, J. G. Analytis, S. Meister, Y. Chen, H.-J. Zhang, I. R. Fisher, Z.-X. Shen, and Y. Cui, ACS Nano **5**, 4698 (2011).

[39] Z. H. Zhu, C. N. Veenstra, G. Levy, A. Ubaldini, P. Syers, N. P. Butch, J. Paglione, M. W. Haverkort, I. S. Elfimov, and A. Damascelli, Phys. Rev. Lett. **110**, 216401 (2013).

[40] Y. H. Wang, D. Hsieh, E. J. Sie, H. Steinberg, D. R. Gardner, Y. S. Lee, P. Jarillo-Herrero, and N. Gedik, Phys. Rev. Lett. **109**, 127401 (2012).

[41] L. A. Wray, S.-Y. Xu, Y. Xia, Y. S. Hor, D. Qian, A. V. Fedorov, H. Lin, A. Bansil, R. J. Cava, and M. Z. Hasan, Nat. Phys. **6**, 855 (2010).

[42] Z. H. Zhu, G. Levy, B. Ludbrook, C. N. Veenstra, J. A. Rosen, R. Comin, D. Wong, P. Dosanjh, A. Ubaldini, P. Syers, N. P. Butch, J. Paglione, I. S. Elfimov, and A. Damascelli, Phys. Rev. Lett. **107**, 186405 (2011).

[43] P. D. C. King, H. M. Bianchi, R. Ovsyannikov, C. Lupulescu, G. Landolt, B. Slomski, J. H. Dil, D. Guan, J. L. Mi, E. D. L. Rienks, J. Fink, A. Lindblad, S. Svensson, S. Bao, G. Balakrishnan, B. B. Iverson, J. Osterwalder, W. Eberhardt, F. Baumberger, and P. Hofmann, Phys. Rev. Lett. **107**, 096802 (2011).

[44] M. Bianchi, D. Guan, S. Bao, J. Mi, B. B. Iversen, P. D. C. King, and P. Hofmann, Nat. Commun. **1**, 128 (2010).

[45] M. S. Bahramy, P. D. C. King, A. de la Torre, J. Chang, M. Shi, L. Patthey, G. Balakrishnan, P. Hofmann, R. Arita, N. Nagaosa, and F. Baumberger, Nat. Commun. **3**, 1159 (2012).

[46] J. Duan, N. Tang, X. He, Y. Yan, S. Zhang, X. Qin, X. Wang, X. Yang, F. Xu, Y. Chen, W. Ge, and B. Shen, Sci. Rep. **4**, 4889 (2013).

[47] M. Bianchi, R. C. Hatch, D. Guan, T. Planke, J. Mi, B. B. Iversen, and P. Hofmann, Semicond. Sci. Technol. **27**, 124001 (2012).

[48] C. Mann, D. West, I. Miotkowski, Y. P. Chen, S. Zhang, and C.-K. Shih, Nat. Commun. **4**, 2277 (2013).

[49] R. V. Aguilar, L. Wu, A. V. S. Stier, L. S. Bilbro, M. Brahlek, N. Bansal, S. Oh, and N. P. Armitage, J. Appl. Phys. **113**, 153702 (2013).

Ambipolar surface state transport in non-metallic stoichiometric Bi_2Se_3 crystals

Paul Syers[1] and Johnpierre Paglione[1, *]

[1] *Center for Nanophysics and Advanced Materials,*
Department of Physics, University of Maryland, College Park, MD 20742

(Dated: October 26, 2016)

A. Materials

In this section we provide further details of our experimental growth techniques. As stated in the main text, a pressurized gas furnace (Morris Research) was used in growing the samples of Bi_2Se_3 measured. Argon gas was used as the pressure medium in the furnace, which is capable of reaching pressures up to 200 bar at 1200°C. The gas was used to pump and flush the furnace chamber, before being sealed off at a controlled pressure before the start of the heating cycle. The pressure of the furnace chamber was continuously monitored during the growth cycle and it was determined that a room temperature pressure of roughly 45 bar consistently produces samples with the lowest carrier concentration. It should be noted that the growth tubes were laid in a nearly horizontal position in the furnace, with a slight vertical angle ($\leq 10°$) and the measured carrier concentration varied monotonically with the part of the growth from which the sample was taken. Growths were heated at rate $\geq 50°$C/h to 750°C, held for a few hours before being cooled at -20°C/h to 650°C, at which point the cooling rate was slowed down significantly and the growths were cooled further to 350°C before the furnace was turned off and allowed to cool at an uncontrolled rate. Quenching in water, from 450°C, was also tested on normal flux growth batches, but that only proved to greatly increase the bulk carrier concentration of the samples. It is assumed this is because at higher temperatures, the Se is much more mobile within the formed crystals, resulting in more Se vacancies, and quenching to room temperature effectively freezes in the higher defect density. Aside from time spent preparing the samples for measurements, all growths and samples were stored at room temperature under high vacuum.

B. Measurements

We provide additional details in this section, pertaining to the behavior of the materials in the measurements discussed in this study. Electrical transport measurements were performed on all samples multiple times over a period of months. Measurements were made from 300 K to 1.8 K and up to ± 14 T. A significant change in the temperature dependence between measurements taken two days apart was observed in some samples, a major sign of the volatility of the chemical potential in undoped Bi_2Se_3. Little ($\leq 10\%$) thermal cycling was seen in sample F during measurements, and none in all other samples. Later measurements taken on the nonmetallic samples a few months after the data shown in the main body of the paper did not show any of the non-metallic behavior in any of the samples. The top plot in Fig. 1 shows the change in resistivity for the samples over time and the two curves for sample A illustrate how rapidly the characteristics of this material can change between measurements taken only 2 days apart. While significant changes in sample quality due to exposure to air have been seen [1, 2], this is evidence that even storage at room temperatures in vaccuum is not enough to prevent such changes.

The longitudinal magnetoresistance (MR) of nearly all samples, shown in the bottom of Fig. 1, follows the strong, quasi-linear MR seen in previously reported low doped samples [3]. While the magnitude of the MR seems to have no correlation with carrier concentration or insulating behavior, Sample A stands out from the others due to its cusp-like behavior at low fields, and its non-linear behavior at high fields. The low field behavior resembles the weak antilocalization cusps previously reported in thin films of Bi_2Se_3 [4], however, fits to the expected WAL behavior fail to correctly describe the behavior.

Scanning electron microscopy and energy-dispersive electron spectroscopy (EDS) measurements were performed on all samples after all transport measurements, showing no sign of multiple phases, twinning, or any other large scale defects. Only signatures of Bi and Se were observed, and the ratios of constituent elements were within experimental error of stoichiometric ratios expected for Bi_2Se_3.

C. Analysis

Here we present our method for obtaining curve fits to the Hall effect data, using a two band model [5], as well as our method for placement of the Fermi energies in bismuth selenide's band structure. The Hall resistance vs field data in Fig. 2 shows significant nonlinear behavior. The data was antisymmetrized, to isolate the ρ_{xy} component. Even after antisymmetrization of the Hall effect data, samples A and F showed strong extreme curvature
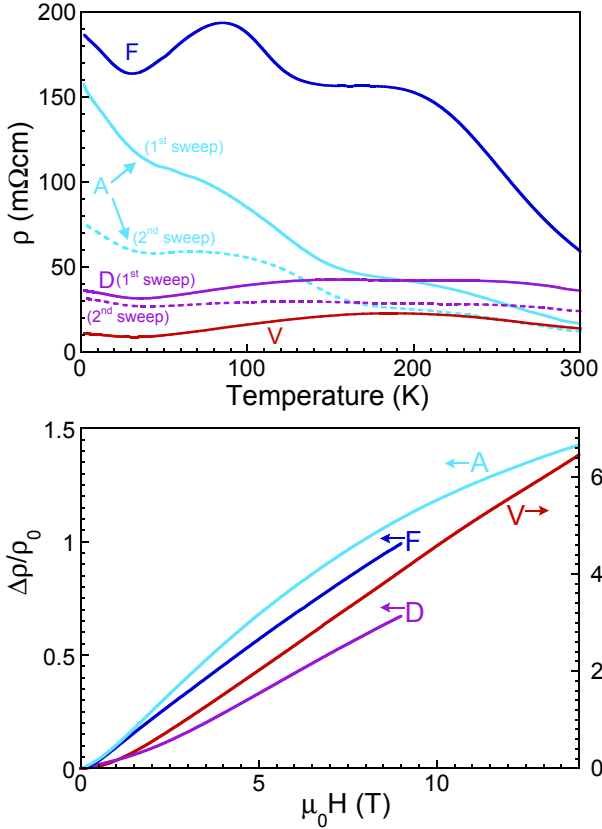

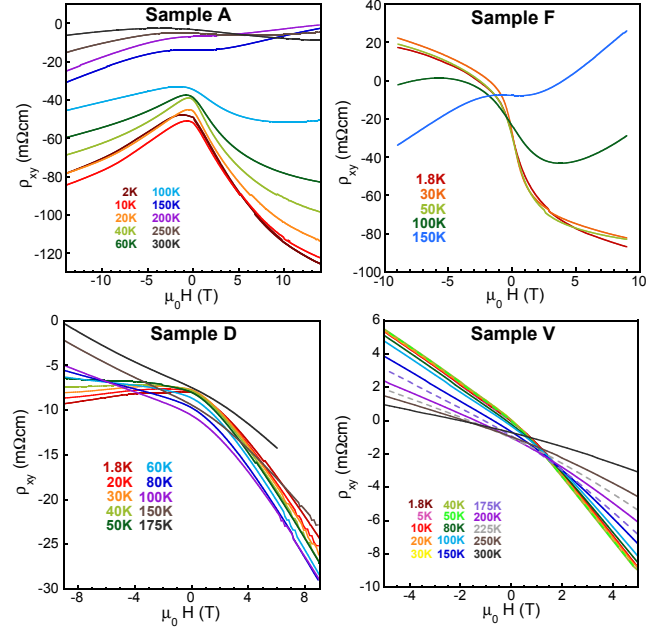*Electronic address: paglione@umd.edu

FIG. 2: Hall resistance vs magnetic field shown for all four samples discussed. Each plot shows all curves taken at different temperatures before applying anti-symmetrization analysis.

and a crossover in the sign of the Hall coefficient.

The following expression of the Drude model was used to fit the symmetrized Hall data

$$\rho_{xy} = \frac{\sigma_h{}^2 R_h - \sigma_e{}^2 R_e - \sigma_h{}^2 \sigma_e{}^2 R_h R_e (R_h - R_e) H^2}{(\sigma_h + \sigma_e)^2 + \sigma_h{}^2 \sigma_e{}^2 (R_h - R_e)^2 H^2} H \quad (1)$$

with σ and R being the conductivities and Hall coefficients of the contributing carrier types - holes and electrons. Given the nearly isotropic, single band nature of the Fermi surface of Bi_2Se_3, the following approximations were applied to the model: $R_i = 1/\eta_i e$, $\mu_i = \sigma_i R_i$ with η, μ being the carrier concentrations and mobilities, respectively and the index i denoting electrons or holes. Using these conversions, we arrive at an expression of the Drude model that depends directly on the carrier concentrations and mobilities of the two types of carriers:

$$\rho_{xy} = \frac{\mu_h{}^2 p - \mu_e{}^2 n - \mu_h{}^2 \mu_e{}^2 (p - n) H^2}{(p\mu_h + n\mu_e)^2 + \mu_h{}^2 \mu_e{}^2 (p - n)^2 H^2} \frac{H}{e} \quad (2)$$

with n and p being the electron and hole carrier concentrations and e being the electron charge. This gives

a five dimensional parameter space for any curve fitting program to explore. Fitting each curve to the model directly produced insufficient and unreliable fits. Fixing the concentration or mobility of one carrier type would help provide a more stable fit, however this introduces nontrivial assumptions about the system. Another analytical method, however, allows a reduction of the parameter space without such assumptions. Equation 2 is of the general form $y = (ax + bx^3)/(c + dx^2)$ which can be re-expressed as a 3rd order polynomial. The polynomial can be solved by a simplified method of least squares fitting: singular value decomposition (SVD). The eigenvectors of the SVD are 4 component vectors; the components corresponding to values of a, b, c, and d. The eigenvector with the eigenvalue closest to zero should contain the values of the coefficients that create the closest possible fit to the data that the Drude model can produce.

While this method provides accurate values of a, b, c, and d, it does not necessarily mean that the physical parameters of carrier concentrations mobilities are obtainable from the fit, but in this case, conversions can be made between the polynomial coefficients and n, p, μ_h and μ_e. It is important to note that the vector containing a, b, c, and d can be modified by a scalar without affecting the accuracy of the fit. Thus, it is not necessarily the individual values of a,b,c, and d but rather the relationships among the parameters that are accurate. This means that for the fits, there is a scalar S that functions as the free parameter and changing S will change the resulting calculations of n, p, μ_e, and μ_h. The resulting

FIG. 1: (Top) Resistivity temperature dependence of four different samples of Bi_2Se_3, with some curves as indicated presenting a second data set measured using the same sample after a time delay (see text). (Bottom) Magnetoresistance of four different samples of Bi_2Se_3. The inset in the bottom graph shows the same data at low fields, highlighting the deviation from H^2 behavior in samples A and D.

parameters are expressed by the following equations.

$$\mu_e = \frac{\sqrt{dS} - aS\sqrt{e} + \sqrt{(\sqrt{dS} - aS\sqrt{e})^2 + 4cS\sqrt{\frac{bSe}{d}}}}{2\sqrt{ct}} \tag{3}$$

$$\mu_h = \frac{\sqrt{\frac{bSe}{d}}}{\mu_e} \tag{4}$$

$$n = \frac{\sqrt{\frac{cS}{e}}\mu_e - \sqrt{\frac{dS}{e}}}{\mu_e{}^2 + \sqrt{\frac{b^2 Se}{d}}} \tag{5}$$

$$p = n + \frac{d}{be} \tag{6}$$

The parameter space of S was explored and a region within these limits was found where all four parameters had reasonable values expected for Bi_2Se_3. The same value of S was used when calculating physical parameters for all data on each sample, but the value of S was allowed to differ from sample to sample. Fig. 3 shows the best obtained values for carrier concentrations and mobilities for all samples discussed. The error bars come from fits using different values of S.

Samples D and V do not show direct evidence of both positive and negative carriers. The small amount of curvature in the data from the two samples is away from the x-axis, not towards it, which is counter to the behavior one would expect from a system with holes and electrons. Thus the two carrier model was adjusted, by changing the sign of the variable p to reflect two bands of the sampe carrier type. The same procedure of SVD and subsequent conversion was successful for the adjusted model. The adjusted model was more accurate in fitting the data from samples D and V than the original model had been. The results from the adjusted model are also shown in Fig. 3.

Samples V and H showed signs of Shubnikov de Haas (SdH) oscillations. The oscillations in sample H have been discussed in the main paper and the oscillations measured in sample V have been plotted in Fig. 4. Modeling of the oscillatory signal using the standard Lifschitz–Kosevich formulism, shown as the solid red line in Fig. 4, can accurately fit the data with only one signal. Shifting of the lowest Landau levels, due to spin orbit coupling [6] causes a change in the oscillation frequency at the highest fields, as seen in Fig. 4b). Early discrepancies between the single frequency model and the data from sample V were resolved when adjusting for this LL-shifting.

The FFT peak was measured to be approximately 19 Tesla, and factoring in the aforementioned LL-shift at higher fields, the actual frequency is closer to 18 T, which
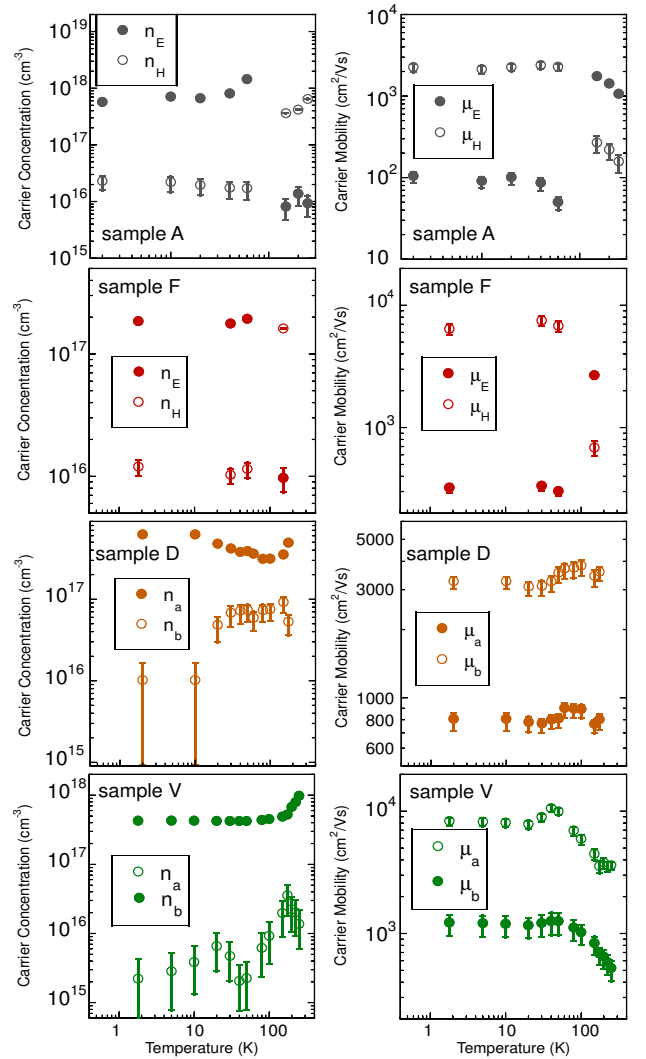

FIG. 3: Two-carrier analysis results yielding carrier concentration (left) and mobility (right) values in all four samples (see text).

corresponds to $n \approx 4.3 \times 10^{17}$ cm^{-3}, matching n_b given by the Drude model. The Dingle temperature given by the model fit corresponds to $\mu \approx 900$ cm^2/Vs, which is close to the value of μ_b from the Drude model. Such close agreement between the SdH oscillations and one band of the two carrier model is strong evidence that the analysis technique is accurate, yet the absence of oscillations from the other band is puzzling. The parameters obtained from the model are listed in Table I. It is important to note the significant difference in phases of the two oscillation signals. Our model of the oscillations fits equally well when setting the phases to exactly π and 0, but it breaks down when the phases are set equal to each other.

While the surface band mobility calculated for sample H from the Dingle temperature is much lower than that given by the Drude analysis, the mobilities for the
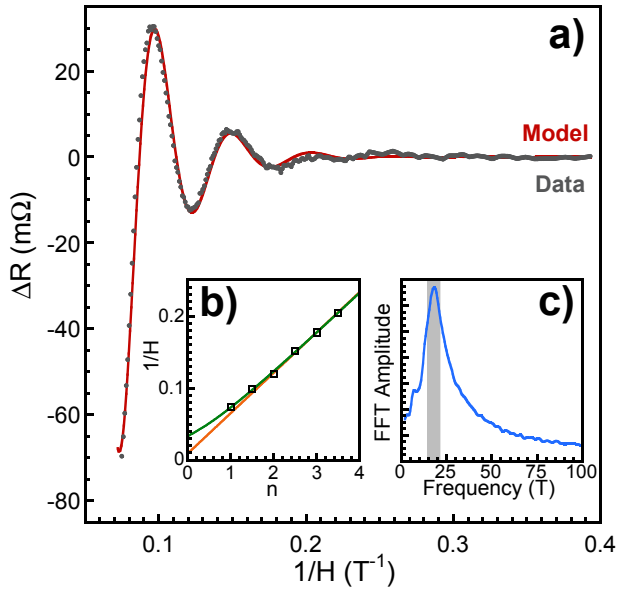
FIG. 4: Quantum oscillations of magnetoresistance of Bi_2Se_3 sample V, plotted as a function of inverse field. The solid red line is a fit to the oscillations using a single frequency model. The inset shows the Fourier Transform of the oscillations, with a single resonance peak indicating the low-frequency plotted in the main figure.

TABLE I: Physical Parameters extracted from Hall and SdH data on a high carrier concentration sample of Bi_2Se_3

	Sample H_a	Sample H_b	Sample V
Drude n ($\times 10^{18} cm^{-3}$)	4.375	5.3	0.427
Drude μ (cm^2/Vs)	7,850	1,250	1,230
SdH n ($\times 10^{18} cm^{-3}$)	4.4	5.3	0.424
SdH μ (cm^2/Vs)	2,660	1,970	1,130
SdH ϕ (rad.)	1.24π	0	0.534π

bulk band are relatively close in value for both samples H and V. Both analyses also show the expected behavior that the carriers at the surface have a higher mobility than those of the bulk. The close agreement of carrier concentrations, as well as the general agreement of mobilities of our two carrier model with the standard analysis method for the SdH oscillations measured in the same sample further confirms the model's validity.

For converting from n to k_f, we used the following standard equation.

$$\mathbf{3D:} k_f = \left(\frac{3N}{\pi}\right)^{1/3} \tag{7}$$

We then used the band structure diagram for Bi_2Se_3- based on ARPES data by Bianchi et. al. [1] to estimate the location of E_F for the surface and bulk states for each sample, given our calculated k_F values and estimated carrier sign. The resultant diagram showing the placement of Fermi energies with respect to the conduction and valence bands is shown in Fig. 4 of the main paper. We use the equation for a 3D fermi space because all carrier concentrations calculated using the Drude model are expressed in cm^{-3}. Any geometric conversions of the concentrations attributed to the surface states would introduce unnecessary uncertainty. Given the orientation of the samples, the k_f of the surface states would be at its maximum value, and therefore the accuracy of the estimates of k_f would not be compromised.

[1] M. Bianchi, D. Guan, S. Bao, J. Mi, B. B. Iversen, P. D. C. King, and P. Hofmann, Nature Communications **1**, 128 (2010).

[2] R. V. Aguilar, L. Wu, A. V. S. an L S Bilbro, M. Brahlek, N. Bansal, S. Oh, and N. P. Armitage, Journal of Applied Physics **113**, 153702 (2013).

[3] N. P. Butch, K. Kirshenbaum, P. Syers, A. B. Sushkov, G. S. Jenkins, H. D. Drew, and J. Paglione, Physical Review B **81**, 241301 (2010).

[4] M. Bianchi, R. C. Hatch, D. Guan, T. Planke, J. Mi, B. B. Iversen, and P. Hofmann, Semiconductor Science and Technology **27**, 124001 (2012).

[5] R. G. Chambers, Proceedings of the Physical Society A **65**, 903 (1952).

[6] A. A. Taskin, Z. Ren, S. Sasaki, K. Segawa, and Y. Ando, Physical Review Letters **107**, 016801 (2011).